JOURNAL OF MATERIALS SCIENCE 23 (1988) 4437–4444

Fracture behaviour of UPVC thin tubes at high loading rates

M. B. JAMARANI*, P. E. REED*, W. R. DAVIES‡
*Departments of * Materials and ‡ Mechanical Engineering, Queen Mary College, Mile End Road, London E1 4NS, UK*

The use of fracture mechanics concepts in describing the failure behaviour of unplasticized poly(vinyl chloride) at high loading rates is studied. An impact test is employed which uses a gas pulse generated by a shock tube to load thin cylindrical specimens. These controlled pulses are used to internally pressurize specimens containing machined notches of different lengths or unnotched specimens. The specimen and the apparatus are both instrumented such that the pressure pulse and the resulting strain in the specimen are monitored throughout the tests to the point of fracture. Linear Elastic Fracture Mechanics (LEFM) is successfully applied to describe the fracture behaviour of the specimens at room temperature over a wide range of loading rates. A criterion is proposed by which the values of K_c and G_c can independently be obtained over the range of the loading rates applied.

1. Introduction

A vital consideration for the use of polymers in engineering applications is the need for their failure behaviour to be known under impact loading conditions. Fracture Mechanics is now applied to a variety of engineering materials including polymers, to relate the applied stress to the maximum permissible flaw size. The technique aims at introducing parameters which identify the fracture criteria for the material under stress. Two different but related approaches to the flaw hypothesis have so far been adopted. Firstly, the energy approach which supposes that fracture occurs when sufficient energy is released as a result of the crack growth to supply that needed to form new fracture surfaces. The fracture energy U_f, measured in conventional Charpy and Izod tests has been found to be strongly dependent on the geometry of the specimen, in particular the crack length. A geometrical factor Φ is therefore introduced such that for the Charpy specimen

$$U_f = G_c BD\Phi \quad (1)$$

where G_c is the critical strain energy release rate, and BD the cross sectional area of the specimen. Values of Φ can be found for various geometries either experimentally or theoretically.

In the second approaching the stress intensity approach, attention is confined to the stress field in the immediate vicinity of the crack tip and the fracture stress σ_f, is related to the initial crack length $2a$ by the following relationship

$$\sigma_f = K_c(Ya)^{-0.5} \quad (2)$$

where K_c is the critical stress intensity factor, and Y a dimensionless parameter that depends on the geometries of the specimen and crack.

Early attempts on the analytical determination of Y in the case of thin cylindrical tubes containing an axial crack, by Folias [1] has produced a relationship of the form

$$\sigma_f = \frac{K_c}{\pi a(1 + C\lambda^2)} \quad (3)$$

where C is a constant depending on crack configuration, and λ a dimensionless curvature parameter. Subsequent experimental examination of Equation 3 proved it to be an accurate representation of the experimental results for values of λ up to 3.4.

In this work a criterion is proposed which allows both K_c and G_c values to be obtained at impact, over a wide range of loading rates.

2. Experimental procedure

Details of the technique used for impact testing the tubular specimens have been described previously [2, 3]. A shock tube is used to apply a well defined impulse to the thin cylindrical specimens of 50.8 mm length, 0.381 mm thickness and 38.1 mm internal diameter, which form an integral part of the shock tube. The specimen is mounted such that it is essentially a freely supported body. Under the action of the internal pressure pulse, the tube can expand radially along its entire length with minimal end restraints. Nominally infinite loading rates (step-loading) are obtained using the experimental arrangement just described in which the shock pulse discharges through the specimen into a dump tank (Fig. 1). The shock tube may also be used to obtain a range of loading rates (ramp-loading), using the same form of specimen mounting arrangements. Modifications required include the addition of a blanking plate at the end of the shock tube and insertion of a nozzle inside the tube just upstream of the specimen support assembly. In this way, the specimen forms a closed volume into which the gas discharges at sonic velocity. The mass

0022–2461/88 $03.00 + .12

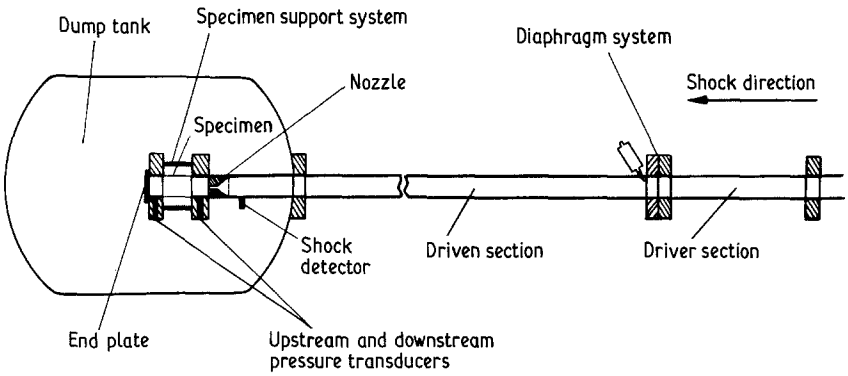

Figure 1 Schematic diagram of the shock tube.

flow rate and consequently the pressurization rate (loading rate) of the specimen is governed by the cross-sectional area of the nozzle and the magnitude of the impulse used. A range of loading rates are obtained by using a selection of different nozzle sizes with various shock pressures.

It should be emphasized that the shock tube technique provides a controlled loading rate test on tubular specimens, in contrast to other testing techniques which provide controlled displacement rates.

An artificial crack of length $2a$ is inserted in the specimen along its generator, using a double-edged sharp scalpel blade. About 270 specimens were subjected to ramp-loading pulses. They were divided into nine sets of constant crack length specimens, each set containing approximately 30 specimens. The specimens of the first set were kept unnotched while those in the other eight were cracked with nominal crack lengths of 1, 2, 3, 4, 5, 6, 8 and 10 mm, thus providing a set of crack length ($2a$) to specimen width (l) ratios of $0.019 < 2a/l < 0.19$. Step type impulses were also applied to a number of both notched and unnotched specimens in which case the shock tube was operated in a reflected shock loading mode [3], i.e. the end of the shock tube blanked causing the shock wave to reflect.

Since the ends of the specimens are open and unrestrained, the strain system acting in the flawed cylinders is considered to be predominantly a unidirectional hoop stress which is given by

$$\sigma_\theta = PR/h \tag{4}$$

where P in the internal pressure, R radius of the cylindrical specimen and h its thickness. The magnitude of the shock pulse is monitored by two piezoelectric pressure transducers with very high frequency response mounted on the shock tube, just beyond each end of the specimen. The strain measurements are carried out by attaching simple rectangular geometry foil resistance gauges onto each specimen. These gauges are attached diametrically opposite to any inserted crack so as not to interfere with deformation in the region of that crack. Therefore, the final record resulting from each test consisted of one (or occasionally two) pressure–time traces corresponding to the transducers on either side of the specimen, and one strain–time trace.

3. Results

3.1. Ramp-loading tests

Typical load–time and strain–time outputs obtained from ramp-loading tests are shown in Fig. 2. By carefully synchronizing the above two traces, at any loading rate the stress–strain behaviour of the specimen may be obtained. Fig. 3 shows the effect of loading

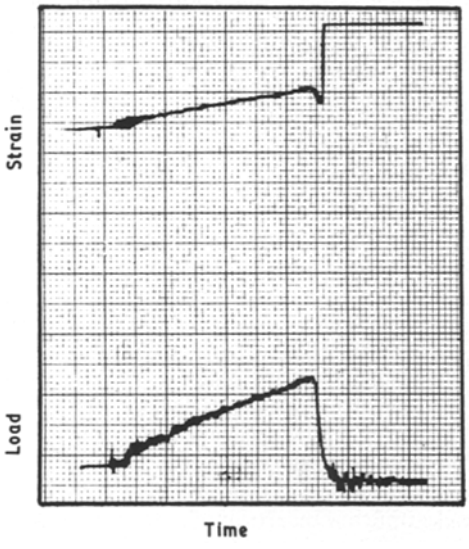

Figure 2 Typical load–time and strain–time traces from ramp-loading tests.

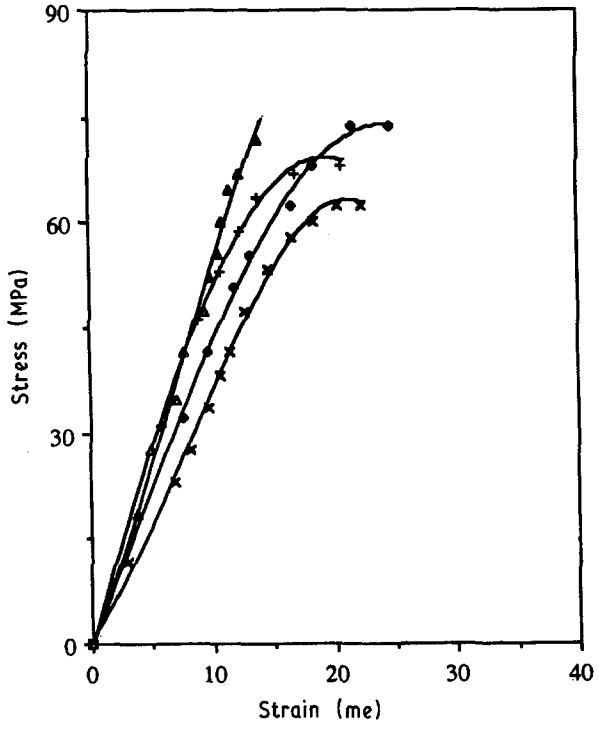

Figure 3 Effect of loading rate (× 1.84 × 10^2 MPa sec^{-1}, ● 3.03 × 10^2 MPa sec^{-1}, + 3.35 × 10^2 MPa sec^{-1}, ▲ 4.67 × 10^2 MPa sec^{-1}) on stress–strain curves of unnotched specimens fractured under ramp-loading.

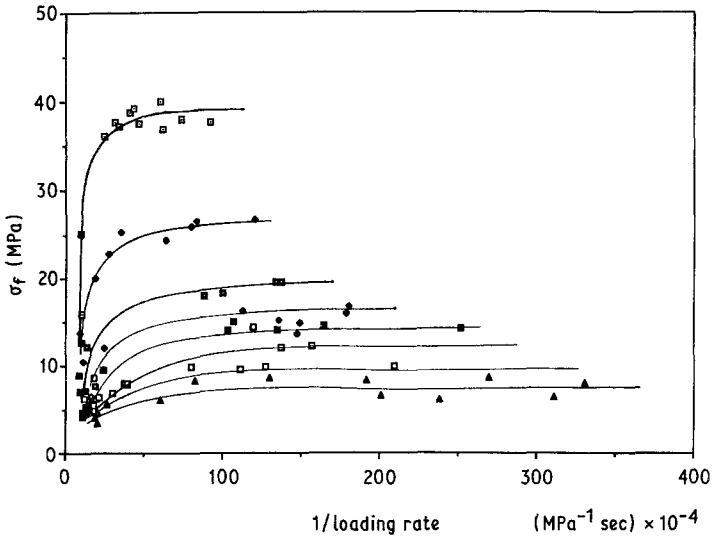

Figure 4 Fracture stress variations with inverse of loading rate for tests on notched specimens with various crack lengths. (⊡ $2a$ = 1 mm, ◆ $2a$ = 2 mm, ■ $2a$ = 3 mm, ◇ $2a$ = 4 mm, ■ $2a$ = 5 mm, □ $2a$ = 6 mm, ▲ $2a$ = 8 mm, △ $2a$ = 10 mm).

rate on the stress–strain curves obtained from tests on *unnotched* specimens. These curves show that

(a) The Young's modulus is increased with increasing rate (i.e. from 3.16 GPa to 3.65 GPa for a range of loading rates extended over one order of magnitude.)

(b) Fracture stress tends to increase slightly with loading rate while the strain to fracture decreases as the loading rate is increased, over the range of the loading rates investigated.

Variations of fracture stress with loading-rate for *pre-notched* specimens with different crack lengths are shown in Fig. 4. In order to facilitate later comparisons with the step-loading data, when the loading rate is nominally infinite and thus difficult to contain in graphical presentation, fracture stress is plotted against the inverse of the loading rate. In this way, the y axis represents the nominally infinite loading rate situation, i.e. the step loading. All curves demonstrate a similar pattern. Namely, the fracture stress σ_f appears to remain independent of the loading rate at relatively low values of the latter (up to 10^2 MPa sec^{-1}), and then drop sharply at very high rates. As might be expected from the fracture mechanics concepts, at each loading rate the values of the fracture stress increases with decreasing crack length. The variations of the fracture stress with nominal crack length may be deduced at any loading rate from the same data. This is shown in Fig. 5 where σ_f is plotted against the non-dimensional crack length $2a/l$ (l is the specimen length), for two extreme values of the loading-rate.

Examination of the dependence of fracture energy (area under the load–displacement curve) on the loading rate shows that it decreases with increasing loading rate for all specimens.

3.2. Step-loading tests

Typical load–time responses of the specimens under both incident and reflected modes of step-loading, are shown in Fig. 6. In both cases the ideal step function obtained initially was followed by a slow pressure rise just prior to the collapse of the specimen. In reflected mode, the specimen was loaded in two distinct steps, albeit at short time separation. The time lapse between the two steps corresponds to the time taken for the shock wave to travel along the length of the specimen and then be reflected back to the measuring transducer, i.e. to travel twice the specimen length since the transducer is mounted close to the start of the specimen. This was verified by comparing the observed time lapse with that calculated, knowing the velocity of the particular shock impulse in the gases used. The strain traces follow the same general pattern as the pressure trace, both being approximately of the step form. However it is noted that in this case, a lightly

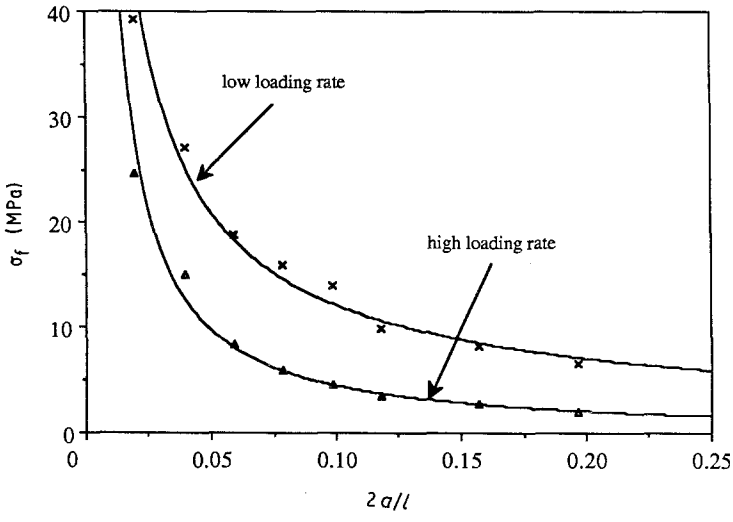

Figure 5 Variations of fracture stress with non-dimensional crack length for two values of loading rate.

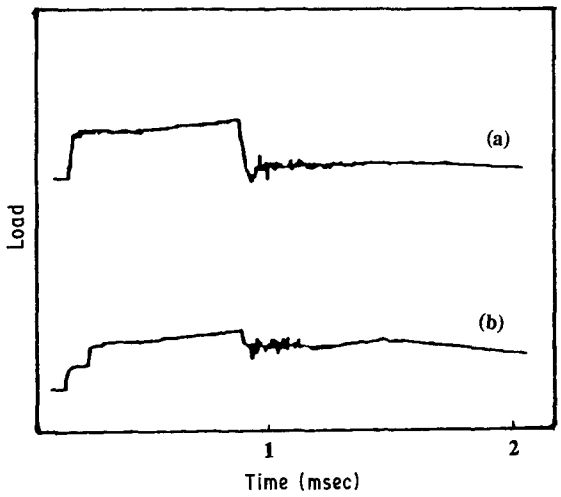

Figure 6 Typical load–time traces for step-loading tests.

damped oscillatory motion is found to be superimposed on the rise in the strain.

A number of tests were carried out on specimens containing cracks of different lengths (between 1 and 10 mm). It was found that increasing the magnitude of the incident shock pressure results in decreasing the time to fracture t_f, while the fracture stress remains constant. This situation arises due to the steady increase in pressure throughout the shock, causing the fracture stress to be achieved at different times. This is schematically shown in Fig. 7. Impulses of varying strengths were applied to the specimens and hence the minimum shock pressure necessary for instantaneous fracture was found (marked as P_f in Fig. 7).

Fig. 8 shows the variations in the minimum value of shock pressure needed for instantaneous fracture, with the non-dimensional crack length, $2a/l$.It is observed that for short cracks, the minimum values of the shock pressure decreases rapidly with increasing notch length. Fig. 8 also indicates that for specimens with longer cracks, the minimum value of shock pressure necessary for fracture decreases only very slightly with increasing crack length.

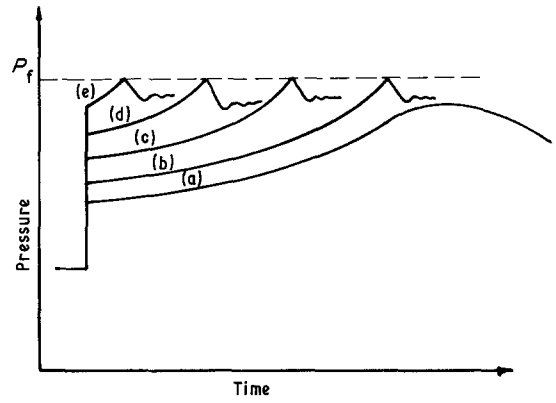

Figure 7 Effect of increase in shock pressure on the fracture stress, σ_f and fracture time, t_f, in step-loading tests (not to scale).

4. Application of LEFM

4.1. Stress intensity approach

According to the generalized flaw theory, there should be a linear relationship between the fracture stress σ_f and the inverse square root of the crack length. Using the results obtained from the ramp-loading tests, values of fracture stress are plotted against $(\pi a)^{-1/2}$ for various rates of loading up to 10^3 MPa sec^{-1}. This is shown in Fig. 9. It can be seen that at any constant loading rate, a linear relationship exists between the measured value of σ_f and the inverse square root of the crack length. The lines, however, do not extrapolate to the origin, giving the following expression for the fracture stress

$$\sigma_f = \frac{K_c}{(\pi a)^{1/2}} + \sigma_\infty \qquad (5)$$

where σ_∞ varies with loading rate.

Previous attempts to eliminate σ_∞ by means of the bending and finite width correction factors and fit the data to a true Griffith equation had not been completely successful [4].

By studying the problem of crack growth in a thin cylindrical shell containing an axial crack of length $2a$ subjected to internal pressure P, Folias [1] solved the

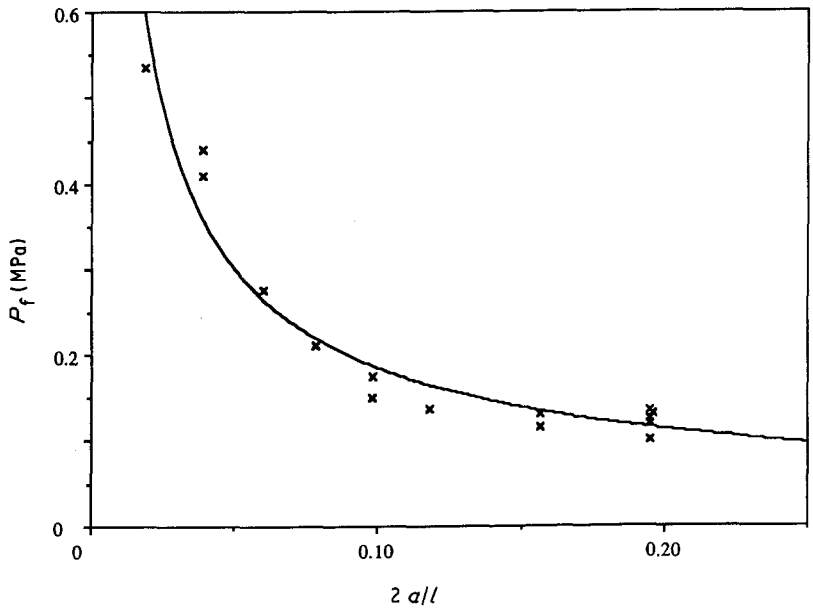

Figure 8 Variations in the minimum initial reflect shock pressure necessary for fracture with non-dimensional crack length, for step-loading tests on notched specimens.

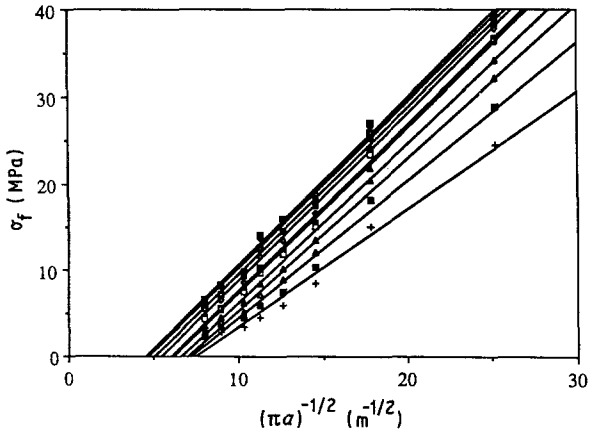

Figure 9 Fracture stress data plotted against $(\pi a)^{-0.5}$ at various loading rates. (□ 100 MPa sec^{-1}, ◆ 125 MPa sec^{-1}, ■ 150 MPa sec^{-1}, ◆ 200 MPa sec^{-1}, ■ 250 MPa sec^{-1}, □ 300 MPa sec^{-1}, ▲ 400 MPa sec^{-1}, ▲ 500 MPa sec^{-1}, ■ 670 MPa sec^{-1}, + 1000 MPa sec^{-1}).

following coupled differential equations governing the displacement function W and the stress function F, with x and y dimensionless rectangular coordinates

$$\frac{Eha^2}{r}\frac{\partial^2 W}{\partial x^2} + \nabla^2 F = 0$$
$$\nabla^4 W - \frac{a^2}{rD}\frac{\partial^2 F}{\partial x^2} = \frac{P}{D}a^4 \quad (6)$$

where D is the bending stiffness of the cylinder wall or, as it is more commonly known, the flexural rigidity. Analytical solution of the above equations provides appropriate values for the resulting extensional and bending stresses. The dimensionless curvature parameter λ is introduced to account for the initial bending effects. In a cracked cylindrical tube under internal pressure alone, this effect may be considered by the following equation

$$\left(\frac{\sigma_{tube}}{\sigma_{plate}}\right)^2 (1 + C\lambda^2) = 1 \quad (7)$$

where C is a constant which depends on the crack configuration and takes a value of 0.49 in the present case (i.e. axial crack). λ is defined by

$$\lambda^2 = [12(1 - \nu^2)]^{1/2}\frac{a^2}{Rh} \quad (8)$$

where ν is Poisson's ratio for the material, R the radius and h the thickness of the tube. Therefore substituting $\nu = 0.42$ for PVC [5], Equation 7 becomes

$$\sigma^2\left(1 + 1.54\frac{a^2}{Rh}\right) = \frac{K^2}{\pi a} \quad (9)$$

where σ is the hoop stress. Hence the following fracture criterion for the specimen is obtained

$$\sigma_f = K_c\left[\pi a\left(1 + 1.54\frac{a^2}{Rh}\right)\right]^{-1/2} \quad (10)$$

This would mean that in the particular case of the thin PVC tubes with axial cracks used in this work, the hoop stress to fracture is a factor of $(1 + 1.54\ a^2/Rh)^{1/2}$ smaller than the uniaxial stress required for the failure in the case of a flat plate of the same material.

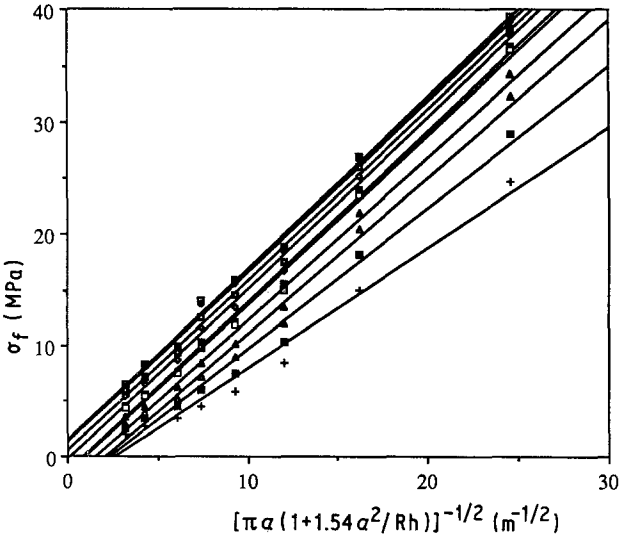

Figure 10 Fracture stress data plotted against $[\pi a(1 + 1.54a^2/Rh)]^{-0.5}$ at different load rates. (□ 100 MPa sec^{-1}, ◆ 125 MPa sec^{-1}, ■ 150 MPa sec^{-1}, ◆ 200 MPa sec^{-1}, ■ 250 MPa sec^{-1}, □ 300 MPa sec^{-1}, ▲ 400 MPa sec^{-1}, ▲ 500 MPa sec^{-1}, ■ 670 MPa sec^{-1}, + 1000 MPa sec^{-1}).

In the present test series, λ takes values between 0.33 and 3.26 resulting in a range of K_t/K_p values between 1.03 and 2.5, where K_t and K_p are stress intensity factors for the tube and equivalent flat plate, respectively.

The same fracture stress data as the ones shown in Fig. 9 are plotted in Fig. 10 over the same range of loading rates, this time against $[\pi a(1 + 1.54\ a^2/Rh)]^{-1/2}$. It is clear from the graphs of Fig. 10 that the use of Folias' factor corrects the data to a large extent, with all the lines now extrapolating closer to the origin. It should be noted that the slope of the lines give values of the critical stress intensity factor at various loading rates, which in the plane strain situation represents fracture toughness, K_{Ic} at that rate. It can be seen that the slopes of the lines increase as the loading rate decreases from 1000 MPa sec^{-1} to around 250 MPa sec^{-1}, but changes less rapidly at lower loading rates. Hence K_c decreases with increasing loading rate, decreasing more rapidly as the higher loading rates are reached. The same analysis may be used to calculate a value for K_c at impact (nominally infinite loading rate), from the step-loading results on notched specimens. This was found to give a K_c value of 1.09 MPa m$^{1/2}$. Values of fracture toughness obtained from the tests on notched samples are plotted in Fig. 11 over the full range of the applied loading rates studied, including step loading.

4.2. Energy balance approach

Various methods are used to determine the strain energy release rate experimentally. One most frequently used is known as the compliance method in which the compliance, the reciprocal of the slope of the load–deflection curve, is measured as a function of the crack length. The technique is described in detail elsewhere [6, 7]. A similar approach may be adopted to determine the geometrical factor, Φ in the case of the thin cylindrical specimens and hence evaluate the critical value of G at instability. It can be shown that the energy absorbed by the specimen at fracture may be

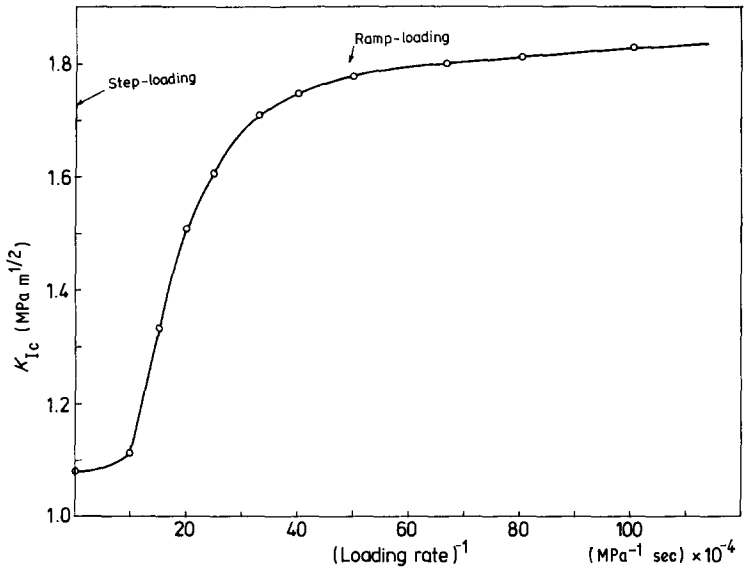

Figure 11 Fracture toughness variations with loading rates up to the step-loading.

expressed as

$$U = Ghl\left(\frac{5.19Rhx^2l + x^4l^3 + 41.56R^2h}{20.78Rhxl + 8x^3l^3}\right) \quad (11)$$

where $x = 2a/l$ and the expression inside the parenthesis is the geometrical factor which can be denoted by Φ. The derivation of this equation is given in the appendix. At fracture U becomes the energy for fracture and G the critical energy release rate, G_c. As expected, a linear relationship is obtained between the fracture energy and the product $hl\Phi$, indicating a constant G_c value at each loading rate. Variations of the critical strain energy release rate with loading rate found from these graphs are shown in Fig. 12. G_c is found to decrease with increasing loading rate, with a descending rate of decrease as the loading rate increases.

If the variations of Young's modulus with the loading rate are known (from ramp-loading tests), an alternative method of measuring G_c is to use the relationship between G and K (i.e. $K^2 = G/E$). A graph of G_c against the loading rate, found in this way is shown in Fig. 13. A reasonably good correlation is obtained between G_c values found by the two techniques.

5. Discussion

Three distinct regions can be recognized in Fig. 11, where values of fracture toughness are shown over the range of the applied loading rates, up to the step-loading for uPVC:

(a) for loading rates below 200 MPa sec^{-1}, fracture toughness is nearly independent of the loading rate maintaining a value of $K_c = 1.81$ MPa m$^{1/2}$.

(b) for loading rates between 200 and 1000 MPa sec^{-1} there is a sharply decreasing fracture toughness with increasing rate, and

(c) finally the fracture toughness appears to tend to a limiting minimum value at loading rates above 10^3 MPa sec^{-1} up to the step-loading.

The decreasing toughness with increasing rate behaviour observed over a large part of the range of the rates used in this work is also noted by several other investigators working on various materials over the same range [8–10]. This is also in accordance with the viscoelastic analysis of the materials response to high loading rate impulses which implies a diminishing viscous effect, and hence a more brittle fracture behaviour at high testing speeds [3].

The existence of two fracture toughness values for a given material has been noticed by other workers (e.g. [11]), explaining these values as a K_{C1} for the state of plane strain which corresponds to the smallest amount of plastic deformation, and K_{C2} for a plane stress system in which there is freedom from lateral constraint and consequently much greater plastic deformation. Similar arguments may be adopted for

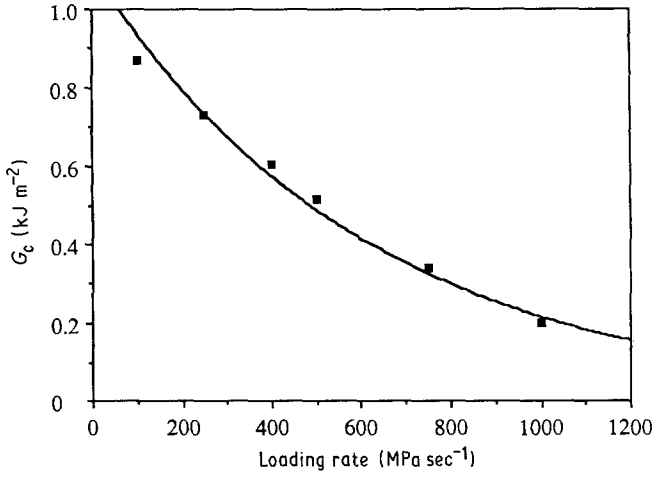

Figure 12 Variations of the critical strain energy release rate with the rate of loading obtained by the energy balance approach.

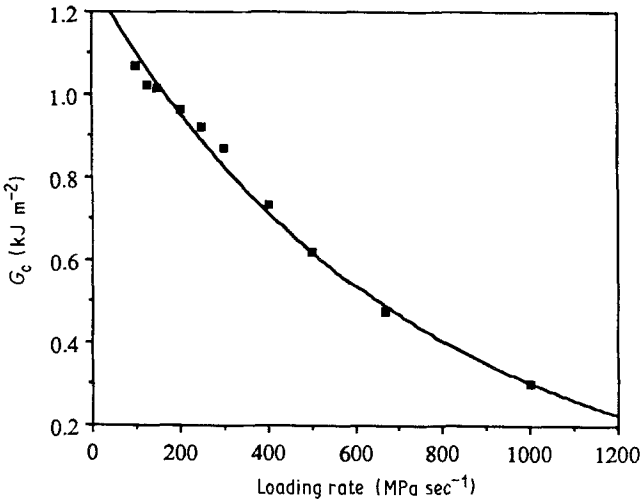

Figure 13 G_c variations with the loading rate by the stress intensity approach.

the results shown in Fig. 11, which will be discussed in a subsequent paper. While two limiting values are observed in the fracture toughness measurements here, however, it must be noted that a large section of the range of the loading rates applied in the present investigation corresponds to the transitional region between the two limiting situations. In this region, as it can be seen, the K_c values decrease as the loading rate is increased.

Many investigators [12–14] have sought to measure the fracture toughness of PVC materials, using different testing techniques. Fig. 14 compares the K_c data obtained from the current experiments with those quoted in the literature. It is difficult to obtain exact comparisons, since the parameters to measure the rate are not always expressed definitively and there are further problems in comparing results from displacement rate controlled tests with those of strain rate. However, it can be seen in general that K_c decreases as the rate is increased.

The fracture toughness results obtained in the present work extend the range of loading rates over which toughness values have so far been obtained for uPVC. The changes observed in the fracture toughness of PVC over the wide range of rates shown in Fig. 14 may be interpreted in terms of the relaxation processes in the material. The influence of relaxation processes on the mechanical properties of polymers is known to be considerable [12]. Correlation between the fracture behaviour and relaxation processes in PVC at two widely different loading rates, under static and impact conditions, have been studied before [12] and a strong rate dependence in the toughness values, has been observed. In Fig. 14, the first transition observed in the results of Darwish *et al.* at low speeds ($\dot{d}$ = 1 mm sec^{-1}), may be attributed to the primary relaxation region associated with the main static transition temperature T_g, while a second relaxation region is observed at a much higher displacement rate ($\dot{d}$ = 1000 mm sec^{-1}). It can be seen that, a reasonably good correlation exists between the present high loading rate tests results with those derived from static tests.

6. Conclusions

The experimental data presented in this paper has shown that the considerations of rate effects in determining fracture parameters in polymers are of paramount importance. The main findings and conclusions are as follows.

(1) The concepts of linear elastic fracture mechanics may be applied with advantage to describe fracture of thin PVC tubes, at high rates of loading.

(2) Folias' analysis for axial cracks in cylindrical shells corrects the data for bending effects and hence plots of σ_f against $(Ya)^{-1/2}$ produced straight lines passing through the origin. The fracture toughness parameter K_c found in this way proved to

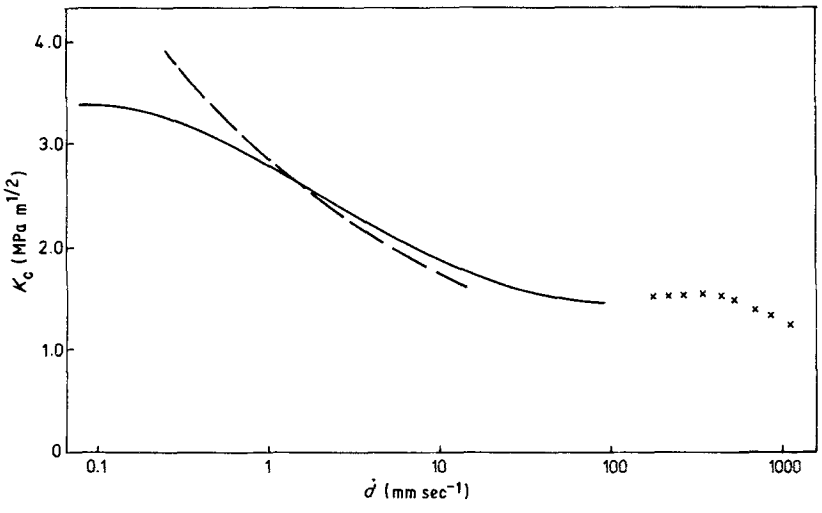

Figure 14 Comparison of the present data (x) with those existing in the literature. (—— Darwish *et al.*, – – – Sweeney *et al.*)

be rate dependent at loading rates higher than 250 MPa sec^{-1}.

(3) The value of K_c appears to vary between an upper bound value of 1.8 MPa $m^{0.5}$ and a lowerbound value of 1.1 MPa $m^{0.5}$ as the loading rate increases, which may be related to a change from plane strain to plain stress conditions determined by the rate of deformation.

(4) A reasonably good correlation was obtained between the fracture toughness found by the stress intensity approach and the energy approach. The calibration factor Φ, previously used for Charpy and Izod impact test analysis could also be adopted to provide a further means of analysing data from the shock tube technique used.

(5) Finally, the shock tube technique is considered to provide a new approach to high speed testing of materials which can lead to further understanding of their behaviour at high rates of loading.

Appendix

The energy balance approach considers the changes in the total energy of a cracked body, and is based on the idea that if, as a result of an incremental crack growth, the decrease in the stored elastic energy of the body is greater than the energy absorbed by forming new crack surfaces, then unstable crack propagation would occur. For unstable failure, the energy absorbed may be expressed as a particular function of crack length, Φ, known as the geometrical factor.

By definition, the strain energy release rate, G is given by

$$G = \frac{1}{h}\frac{dU}{da} \tag{A1}$$

where h in the thickness, U the total energy and a, the semi-crack length. Also the strain energy release rate and stress intensity factor are related by

$$G = \frac{K^2}{E} \tag{A2}$$

and

$$K^2 = \sigma^2 Y^2 a \tag{A3}$$

where E is Young's modulus and Y a geometrical correction factor. Equations A1–A3 give the relationship

$$\frac{dU}{da} = \frac{h\sigma^2 Y^2 a}{E} \tag{A4}$$

integrating this gives

$$U = \int \frac{h\sigma^2 Y^2 a}{E}\,da + U_0 \tag{A5}$$

where U_0 is the stored energy in the specimen of zero crack length given by

$$U_0 = \text{stress} \times \text{strain} \times \text{volume} = \frac{\pi l R h \sigma^2}{E} \tag{A6}$$

Also, from Equations A2 and A3 it can be shown that

$$\frac{\sigma^2}{E} = \frac{G}{Y^2 a} \tag{A7}$$

From Equations A5, A6 and A7

$$U = \frac{Gh}{Y^2 a}\left(\int aY^2 da + \pi l R\right) \tag{A8}$$

But from the Folias' analysis (Equation 9) and Equation A3 we have

$$Y^2 = \pi\left(1 + 1.54\frac{a^2}{Rh}\right) \tag{A9}$$

which by substitution into Equation A8 and carrying out the integration, gives

$$U = Ghl\left(\frac{5.19Rhx^2 l + x^4 l^3 + 41.56R^2 h}{20.78Rhxl + 8x^3 l^3}\right) \tag{A10}$$

where $x = 2a/l$ is the non-dimensional crack length.

In Equation A10, the expression inside the parentheses is the geometrical factor denoted by Φ.

References

1. E. S. FOLIAS, *Int. J. Frac. Mech.* **1** (1965) 104.
2. P. E. REED, P. J. NURSE and E. H. ANDREWS, *J. Mater. Sci.* **9** (1974) 1977.
3. M. B. JAMARANI, PhD thesis, University of London (1986).
4. H. V. SQUIRES and P. E. REED, *J. Mater. Sci.* **10** (1975) 1465.
5. R. SMITH, PhD thesis, University of London (1980).
6. G. P. MARSHALL, J. G. WILLIAMS and C. E. TURNER, *J. Mater. Sci.* **8** (1973) 949.
7. H. R. BROWN, *ibid.* **8** (1973) 941.
8. A. Y. DARWISH, J. F. MANDELL and F. J. McGARRY, *J. Vinyl Tech.* **3** (1981) 246.
9. R. W. E. SHANNON and A. A. WELLS, *Int. J. Fract.* **10** (1974) 471.
10. J. SWEENEY, R. A. DUCKETT and I. M. WARD, *J. Mater. Sci.* **20** (1985) 3605.
11. J. G. WILLIAMS, "Advances in Polymer Science", Vol. 27 Springer-Verlag, Berlin (1978) p. 67.
12. J. C. RADON, *Polym. Engng Sci.* **12** (1972) 425.
13. J. F. MANDELL, A. Y. DARWISH and F. J. McGARRY, *Polym. Engng. Sci.* **22** (1982) 826.
14. J. F. MANDELL, D. R. ROBERTS and F. J. McGARRY, *ibid.* **23** (1983) 404.

Received 9 October 1987
and accepted 10 February 1988